Journal of Civil Engineering and Environmental Technology
Print ISSN: 2349-8404; Online ISSN: 2349-879X; Volume 2, Number 12; April-June, 2015 pp. 86-92

http://www.krishisanskriti.org/jceet.html

Analytical Solutions for Predicting Underwater Explosion & Bubble Phenomena

Anupam Ghosh[1] and Kaushik Bandyopadhyay[2]

[1]Student, Department of Construction Engineering, Jadavpur University, Kolkata
[2]Department of Construction Engineering, Jadavpur University, Kolkata
E-mail: [1]anupamghosh91@gmail.com, [2]kb@const.jusl.ac.in

Abstract—*This study describes different analytical models that have previously been developed for predicting the radial growth and collapse of underwater explosion gas bubbles in a free-field environment. This is done by comparing computational results produced by various reduced model equations. The report describes the implementation of nine analytical gas bubble models, in the form of nonlinear differential equations, and a fourth-order Runge-Kutta solution method. This bubble is modelled using a Lagrangian mesh. Multiple Euler domains are used to the air inside the cylinder, the surrounding air, water and the explosive. Since the model includes air, water and explosive, a multimaterial Euler solver is required. Gas bubble radius time histories calculated with these models are compared to empirical models derived from published experimental data. Comparisons with empirical and theoretical formula are performed in order to corroborate the numerical result.*

Keywords: *Shock wave, radial growth, incompressible fluid, compressible fluid, Runge-Kutta method, adiabatic charge constant, energy loss function.*

1. INTRODUCTION

The early work on underwater explosion based on the bubble dynamics. The detonation of a mass of explosive beneath the ocean surface causes a complex sequence of physical phenomena to occur. If the detonation occurs at the centre of the explosive, a detonation wave then propagates to the surface of the explosive where it meets the surroundings water. The detonation wave is an approximately spherical volume of gas as the explosion bubble.

This project examines various analytical models that are available for predicting the gas bubble growth and collapse. The similitude equations for explosive materials have been shown to provide good results for various shock parameters, such as the peak pressure, decay time, and energy as well as the gas bubble period and maximum free-field gas bubble radius. Major limitations of the similitude equations and current analytical approaches are they do not include effects of loading from the gas bubble collapse, they do not account for the close proximity of a structure and they require an extensive set of constants which depend on the charge material, which can be very difficult to obtain. Another issue with the similitude equations and incompressible fluid analytical models is the lack of energy loss predictions.

From the mechanical point of view, the underwater explosion bubble can be assimilated to an oscillator, consisting of a spring mass system where the internal gas is represented by the spring and the surrounding water by the mass. The spring is initially compressed and will exhibit several pulsations with damping phenomena (mainly due to acoustic radiation and turbulent vertical motion) before reaching the free surface and spreading in the air medium.

2. THEORETICAL ANALYSIS

In the case of a pressure-driven gas bubble initiated near a rigid infinite wall in an incompressible fluid. In this work, surface tension effect was not taken into account because of the generally large size of the gas bubbles. Viscous effects are also neglected because the timescale for viscous diffusion is much larger than the oscillation period for these bubbles. In addition, a rectangular coordinate system O-xyz was adopted with the origin located at the centre of the initial spherical bubble and the z-axis pointing in the opposite direction to gravity. The boundary of the bubble is denoted as S_b, which is a regular surface before and after the jet impact. The fluid domain is denoted by O and it is transformed from a singly connected to a doubly connected region during jet impact.

We assume that the bubbles only contain a non-condensable gas, which can be described as ideal and the expansion and compression of this gas as adiabatic. The internal bubble pressure, P,as a function of the bubble volume, V, is

$$P = P_c + P_0(^{V_0}/_{V})^{\gamma} \quad (1)$$

Where

P_c = the constant vapour pressure inside the bubble

P_0 = the partial pressure due to non-condensing gas

V_0 = the volume of the bubble at P_0

γ = the ratio of specific heats

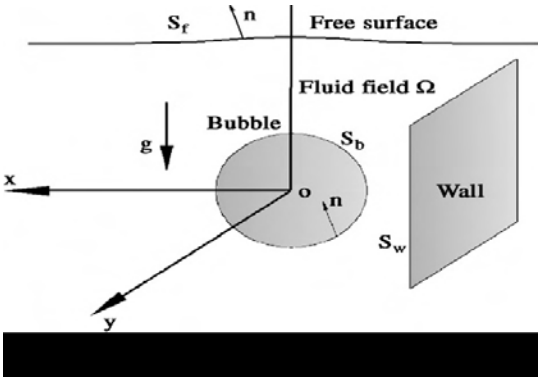

Fig. 1: Coordinate System

The fluid is assumed to be incompressible and the flow irrotational, the velocity potential φ is governed by the Laplace Equation:

$$\nabla^2\phi = 0 \tag{2}$$

Now the velocity, u, anywhere in the flow can be written as

$$U = \nabla\varphi \tag{3}$$

BEM: The Laplace equation is an elliptic equation, so the solution can always be computed everywhere in the fluid domain, provided that either the potential, φ (Dirichlet condition) or the normal velocity, δφ/δn (Neumann condition) is given on the boundaries of the problem. Here δ/δn is the normal inward derivative from the boundary, S, and n is directed out of the fluid, applying the boundary condition at infinite distance '∞'

$$r = \sqrt{x^2 + y^2 + z^2} \to \infty, \phi = 0 \tag{4}$$

Where r = (x, y, z) is the position vector. The boundary-integral equation can be written as

$$\lambda\phi(\mathrm{P}) = \iint_s \left(\frac{\delta\phi(q)}{\delta n}G(p,q) - \phi(q)\frac{\delta}{\delta n}G(p,q)\right)d\,S \tag{5}$$

This equation is Green's integral formula, where S is boundary surface including the bubble surface S_b, the free surface S_f, and the wall surface S_w; p and q are fixed particle and integral variable on boundary surface S, respectively; λ is the solid angle viewed from the point p. λ = 4π when the point p is located inside the flow field, λ = 2π when the point p is located on the smooth boundary surface, and λ< 4π when the point p is located on the corner. The solid angle subtended at the governing point p can be obtained through integral as follows:

$$\lambda = \iint_s \frac{\delta G}{\delta n}(p,q)d\,S, p \in S, \tag{6}$$

G (p, q) is the free-space Green's function for the Laplace equation, which is governed by

$$G(p,q) = |p-q|^{-1} \tag{7}$$

3. EMPIRICAL MODELS

3.1 Similitude Equation

The similitude equation for the first maximum bubble radius is as shown in Eq. (8)

$$R_{\max} = K_6\left(\frac{W}{D+10}\right)^{1/3} \tag{8}$$

R_{max} = maximum bubble radius in meters

D = the charge depth in meter

W = the charge weight in kilograms

K_6 = constant depending upon the charge material

The first bubble period, T_b, in seconds is estimated by Eq. (9):

$$T_b = K_5\frac{W^{1/3}}{(D+10)^{5/6}} \tag{9}$$

K_5 = constant depends on the charge material

$$\Delta d = 12.4\frac{W}{(D+10)} \tag{10}$$

Δd = rise in the gas bubble period

This should be noted that this equation is specific to TNT

The volume of the gas bubble can be reasonably approximated by a half sine function.

$$V(t) = V_0 + (V_{\max} - V_0)\sin\left(\frac{\pi t}{T_b}\right) \tag{11}$$

$$V_{\max} = \frac{4}{3}\pi R_{\max}^{\ 3}$$

V_0 = the initial charge volume

V_{max} = maximum bubble volume

From this volume time relation of the bubble, we can determine the radius time history of a gas bubble by

Eq. (12). $$R(t) = \left(\frac{3}{4\pi}V(t)\right)^{1/3} \tag{12}$$

The vertical position of the gas bubble centre, which describes its vertical migration, can be approximated by Eq. (13).

$$z(t) = -d + \Delta d\left(1 - \cos\left(\frac{\pi t}{2T_b}\right)^{0.4}\right) \tag{13}$$

3.2 Similitude Model with Energy Loss

This approach used the first cycle period constants with an energy loss function to determine the radial and migration time histories. The energy loss function, given by Eq. (14), was provided by van Aanhold, which was based on reduction values used by Geers and Hunter.

$$\lambda = 0.2575 + (1 - 0.2575)\exp(-0.8148m) \qquad (14)$$

Here λ has an initial value of 1 (m=0), and m is the cycle number starting at 0 for detonation and with m=1 for the first gas bubble minimum. The energy loss function is implemented by reducing the charge mass at each gas bubble minimum, such that the new charge weight is λW. This new charge weight is input into Eqs. (8) and (10) to determine the maximum gas bubble radius, the bubble period, and the migration during the next cycle. This energy loss function results in a decrease in the maximum gas bubble radius and periods by an order of ($\lambda^{1/3}$).

3.3Experimental fit model

The average similitude constants for the charge material used in this study are shown in Table 1

Table 1: Demand and deficit for users in command

Constant	TNT		
	1st Cycle	2nd Cycle	3rd Cycle
K5	2.11	1.57	1.33
K6	3.36	2.27	1.76

The three sets of constants for TNT are based on an experimental study by Swift and Decius, who experimentally measured the radius and period of the gas bubble. The similitude constants were determined as the values producing the best fit to the experimental data. For some experiments the fits were produced for the first three bubble periods, but for most experiments there were only measurements for the first one or two bubble periods.

4. ANALYTICAL MODELS

4.1 Introduction

Analytical expressions have been derived for predicting the time history of the gas bubble radius and vertical position. Although several approaches are available there are limitations in the predictive models. Like the similitude equations, the analytical models do not predict the influence of a close proximity target. The various equations of motion (EOM) compared in this paper.

4.1.1 Lamb EOM

$$a\ddot{a} + \frac{3}{2}\dot{a}^2 = \rho_w^{-1}\left(\mathrm{P}_{gas} - \mathrm{P}_{air} + \rho_w g z\right) \qquad (15)$$

4.1.2 Herring EOM (1941)

$$a\ddot{a}\left(1 - 2\frac{\dot{a}}{c_1}\right) + \frac{3}{2}\dot{a}^2\left(1 - \frac{4}{3}\frac{\dot{a}}{3c_1}\right) = \frac{1}{\rho_1}\left(p_g - p_{hyd} + \frac{a}{c_1}\dot{\rho}_g\right) \qquad (16)$$

4.1.3 Krikwood and Bethe (1942) & Brinkley and Krikwood (1950) EOM.

$$a\ddot{a}\left(1 - \frac{\dot{a}}{c_1}\right) + \frac{3}{2}\dot{a}^2\left(1 - \frac{\dot{a}}{3c_1}\right) = \frac{1}{\rho_l}\left(p_g - p_{hyd} + \frac{a}{c_1}\dot{p}_g\right)\left(1 + \frac{\dot{a}}{c_1}\right) \qquad (17)$$

4.1.4 Keller and Kolodner (KK) EOM(1956 a,b).

$$a\ddot{a}\left(1 - \frac{\dot{a}}{c_1}\right) + \frac{3}{2}\dot{a}^2\left(1 - \frac{\dot{a}}{3c_1}\right) = \frac{1}{\rho_l}\left[\left(p_g - p_{hyd}\right)\left(1 + \frac{a}{c_1}\dot{p}_g\right)\left(1 + \frac{\dot{a}}{c_1}\dot{p}_g\right)\right] \qquad (18)$$

4.1.5 Geer and Hunter DA EOM (2002).

$$a\ddot{a} + \frac{3}{2}\dot{a}^2 = \rho_w^{-1}\left(\left(1 + \frac{\dot{a}}{c}\frac{d}{dt}\right)\mathrm{P}_g - \left(\mathrm{P}_{air} - \rho_w g z\right)\right) \qquad (19)$$

4.1.6 Geer and Hunter DAA EOM (2002)

$$a\ddot{a}\left[1 + \zeta - \frac{\dot{a}}{c_1}\left(1 - \frac{\rho_g}{\rho_l}\right)\right]\ldots + \frac{3}{2}\dot{a}^2\left(1 + \frac{2}{3}\zeta - \frac{1}{3}\frac{\dot{a}}{c_l} + \frac{1}{3}\frac{\rho_g}{\rho_l}\right) \qquad (20)$$

$$\left(1 + \frac{\dot{a}}{c_l} + \frac{a}{c_l}\frac{\dot{\rho}_g}{\rho_l}\right)\Big] + a\left(\zeta c_l + a\dot{\zeta}\right)\ldots.$$

$$= \frac{1}{\rho_l}\left[\left(p_g - p_{hyd}\right)\left(1 + \frac{\dot{a}}{c_1}\right) + \frac{a}{c_1}\dot{p}_g\right)\Big]$$

4.1.7 Modified Geers-Hunter (TNO) EOM.

$$\left(\frac{3}{5}W + 4\pi\rho_w a^3\right)\ddot{a} = -6\pi\rho_w a^2\dot{a}^2 + K\pi\rho_w a^2\dot{z}^2 + 4\pi a^2\left(\left(1 + \frac{\dot{a}}{c_l}\frac{d}{dt}\right)P_g - P_{air} + \rho_w g z\right) \qquad (21)$$

$$\left(W + \frac{2}{3}\pi\rho_w a^3\right)\ddot{z} = \left(\frac{4}{3}\pi\rho_w a^3 - W\right)g - 2\pi\rho_w a^2\dot{a}\dot{z} + \frac{\pi}{2}\rho_w C_D a^2\dot{z}\left|\dot{z}\right| \qquad (22)$$

4.2 Equation of state

4.2.1 Similitude Equations

The similitude equations provide three approaches for calculating the radial and migration motion time histories with Eqs. (11) through(13). For the experimental cases which did not have best fits for the first three gas bubble cycles, the average values shown in Table 1 were used. This approach produces results that are very close to, and can be considered to be identical to, the experimental measurements.

4.2.2 Analytical equations of motion

The EOM for the analytical models in Eqs. (15) through (22) are nonlinear second-order differential equations that need to be solved by numerical integration. If the EOM can be expressed in the first order form $y = f(y,t)$, the numerical solution is obtained using a fourth-order Runge-Kutta method, which has the basic form as shown in Eqs. (23) and (24)

$$y_{i+1} = y_i + \Delta t\left[\frac{1}{6}f(y_i,t_i) + \frac{1}{3}f(y^*_{i+1/2},t_{i+1/2}) + \frac{1}{3}f(y^{**}_{i+1/2},t_{i+1/2}) + \frac{1}{6}f(y^*_{i+1},t_{i+1})\right] \qquad (23)$$

Where $y_i$is the variable at the start of the time step, $\Delta t$is the time step, and $f(y,t)$ is the first order differential variable evaluated at y and t.

$$y^*_{i+1/2} = y_i + \frac{\Delta t}{2} f(y_i, t_i)$$
$$y^{**}_{i+\frac{1}{2}} = y_i + \frac{\Delta t}{2} f(y^*_{i+1/2}, t_{i+1/2}) \quad (24)$$
$$y^*_{i+1} = y_i + \Delta t f(y^{**}_{i+\frac{1}{2}}, t_{i+\frac{1}{2}})$$

A second order differential equation (DE) is reduced to a series of first order DEs by creating a dummy variable, in this example *q*, identical to the radial velocity of the gas bubble. The dummy variable is substituted into the original DE. Eq. (25) shows how this is done to produce two first order equations for the Lamb EOM.

$$f_1(q,t) = \dot{q} = \frac{1}{a}[\rho_w^{-1}(p_{gas} - p_{air} + \rho_w g z) - \frac{3}{2}q^2]$$
$$f_2(q,t) = \dot{a} = q \quad (25)$$

For the compressible fluid models the energy loss is inherent within the EOM, so there was no additional energy loss mechanism considered for this study.

4.2.3 Constant

The Swift and Decius report gives no indication of the charge density or any other material properties other than the charge type. For this reason two sets of charge constants were used for comparison purposes. The constants used for the analytical models are shown in Table 2

Table 2: Constants used for solving the analytical models

Variables		Set 1	Set 2
Explosive Density (kg/m3)		1500	1630
Gas exponent		1.25	4/3
Adiabatic charge Constant (MPa), K	Compressible	1350	2455
	Incompressible	740	1050
Drag Coefficient, Cd		2.25	2.25
Density of seawater (kg/m3)		1025	1025
Sound velocity in water (m/s)		1500	1500
Acceleration of gravity (m/s2)		9.80665	9.80665
Air pressure (kPa)		101.325	101.325

5. RESULTS AND ANALYSIS

5.1 Similitude Model

The approach uses the experimental results published by Swift and Decius to directly calculate the radius and period of each bubble cycle, referred to as the "Exp. Fit" model. At the first gas bubble minimum the similitude constants are changed to the values for the second cycle. The same approach is used at the second gas bubble minimum. For the experimental cases which did not have best fits for the first three gas bubble cycles, the average values shown in Table 1 were used.

5.2. Similitude Energy Loss Model vs. Experimental Fit Model

Fig. 2 shows a comparison of the experimental measurements and the energy loss function used in conjunction with the similitude equations.

From Fig. 2 it can be seen that the energy loss function does not provide the required amount of reduction in the bubble period or radius. The energy loss function will result in a period and radius reduction of approximately 16 percent for the second bubble cycle and an additional 10 percent for the third bubble cycle. From the experimental fit it was found that on average the gas bubble period is reduced by approximately 25 percent and another 11 percent over the first and second bubble cycles respectively. The bubble radius over the first and second bubble cycles are reduced by 32 and 15 percent.

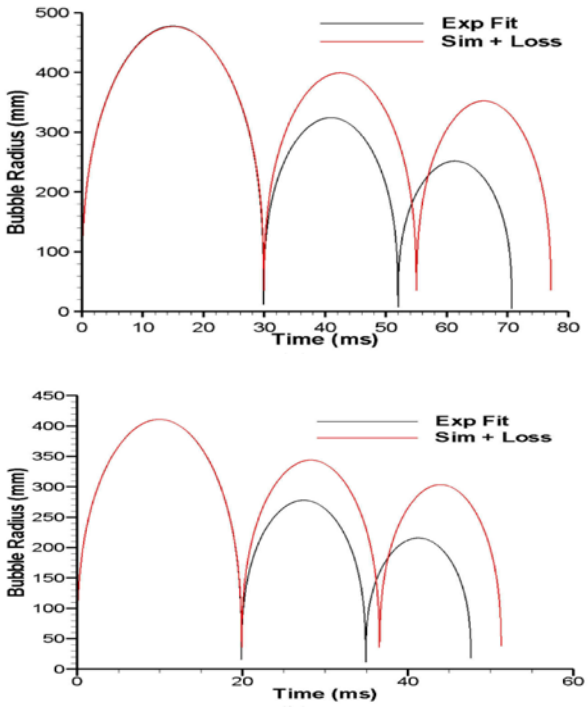

Fig. 2: Comparison of experimental similitude response and similitude with energy loss (function (a) Case G5F (b) Case G70F)

5.3 Analytical Models

The following sections compare the bubble radius time history for the various analytical models, including the effect of fluid compressibility and the charge properties on the radius time history. Fig. 3(a) shows a typical gas bubble migration time history. Due to the small bubble migration, less than 1 percent of the total depth, the coupling of bubble depth and radius had a negligible effect on the gas bubble radius time histories, as shown by Fig. 3(b).

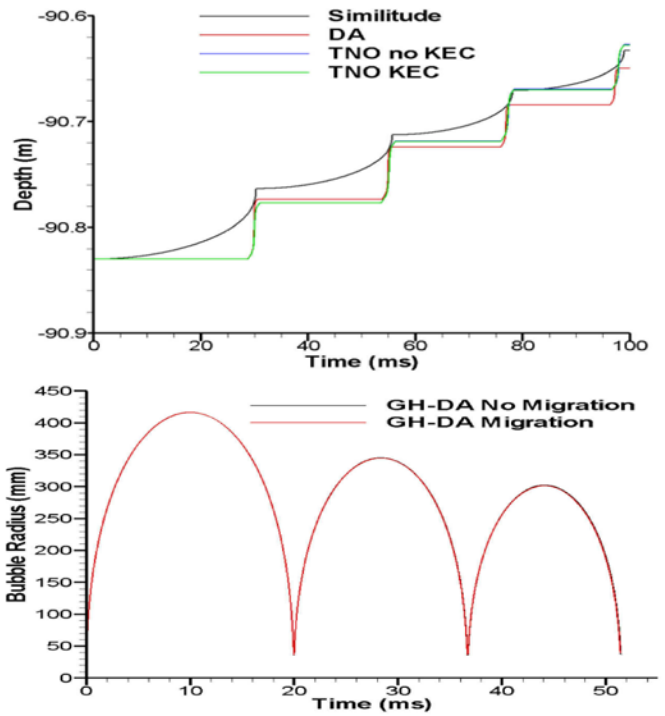

Fig. 3: Effect of including bubble migration in the analytical model (a) Typical gas bubble migration (b) Radius for a migration + dilatation model and dilatation only

5.4 Effect of Fluid Compressibility

Fig. 4 shows the bubble radius time history of all analytical models for the depth and charge size for test case G5F. Fig. 4(a) shows that all compressible gas models reduce to the Lamb EOM when the fluid becomes incompressible. Fig. 4(b) shows a comparison of all the analytical models with the water considered as a compressible fluid, with the exception of the Lamb EOM which does not have any compressible fluid modelling capability. These results are grouped according to compressibility. Considering just water compressibility the various models show little variation for a detonation depth of 93 m. The only models that show a significant difference are the Lamb EOM which does not consider water compressibility and the Geers-Hunter DAA (GH-DAA) model which includes compressibility in the water and the gas bubble. The additional energy loss factors considered in the GH-DAA formulation significantly reduces the maximum gas bubble radius and period when compared to the other analytical approaches.

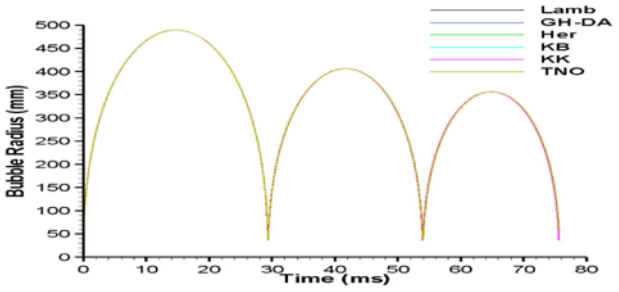

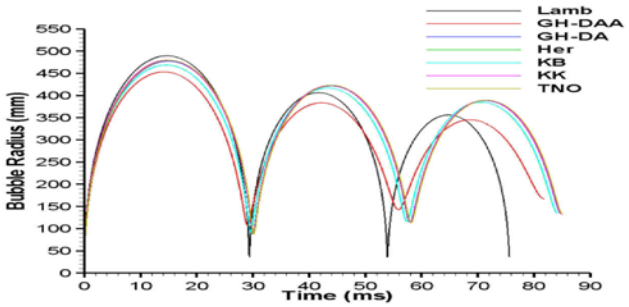

Fig. 4: Comparison of analytical bubble radius time history for a charge size and detonation depth equivalent to test G17F(a) Incompressible Fluid (b) Compressible Fluid

5.5 Analytical Models vs. Experimental Fit Model.

Fig. 5 through Fig. 8 compares analytical models with experimental fit results. GiF indicates the use of the similitude constants for the *ith*test number from Swift and Decius. Exp Fit indicates the experimental fit constants for all three bubble cycles are used. Sim + Loss indicates the first bubble cycle similitude constants are used along with the energy loss function. For the analytical models it is the name of the model followed by the property set from Table 2, where Prop1 indicates property set 1 and Prop2 is for property set 2.

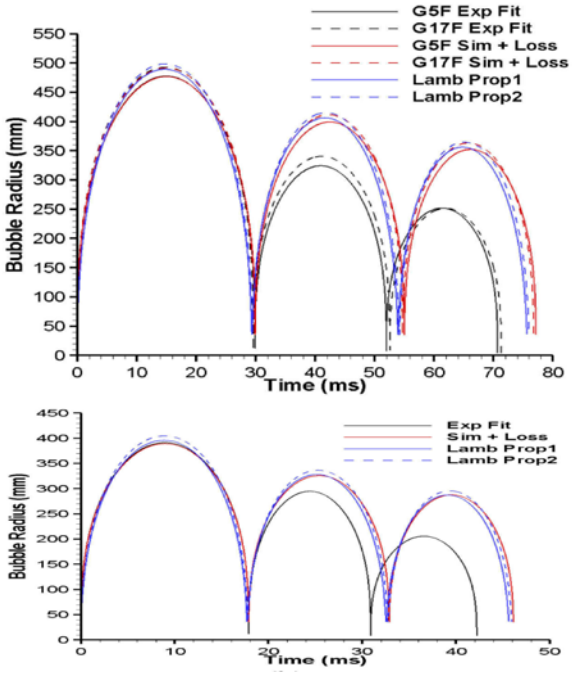

Fig. 5: Comparison of experimental similitude response and the Lamb EOM with energy loss function (a) 93 m depth (b) 179 m depth

From Fig. 5 it can be seen that the general behaviour of the Lamb EOM follows that of the similitude equation, with a slight improvement in the bubble period predictions for the Lamb EOM. The same energy loss function is applied to both of these models. The energy loss function does not provide the

required energy reduction for the Lamb EOM as the peak radii and bubble periods of the experimental fits are significantly less.

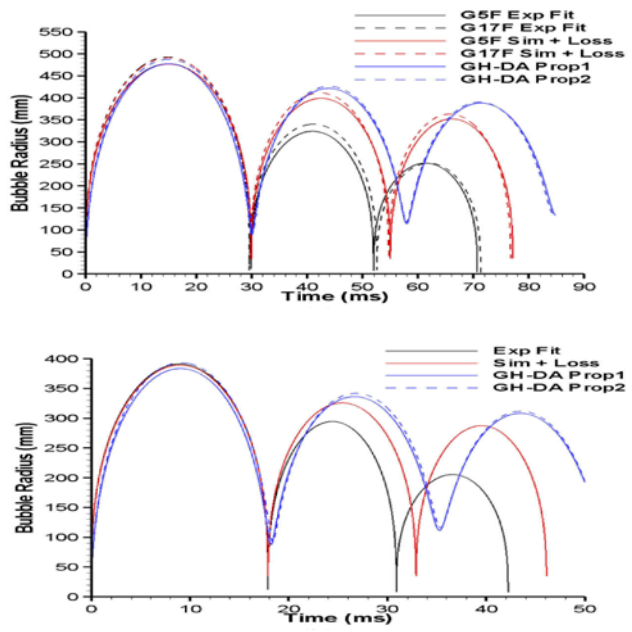

Fig. 6: Comparison of experimental similitude response and the GH-DA EOM (a) 93 m depth (b) 179 m depth

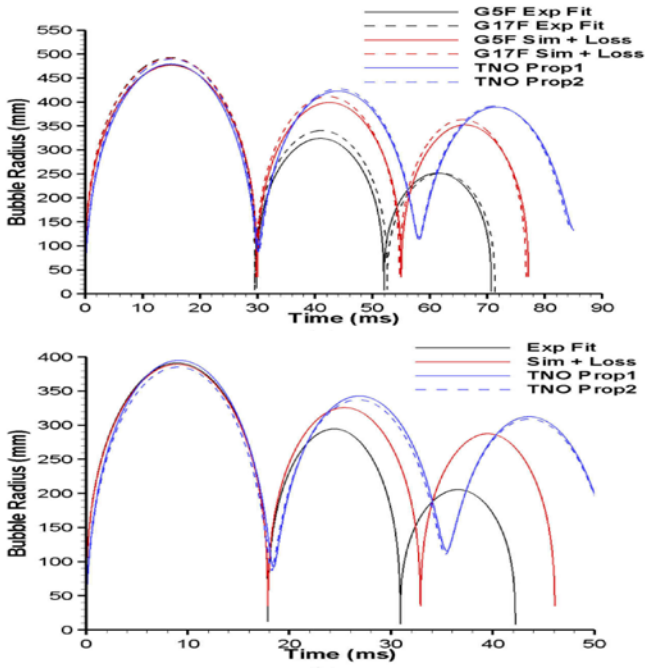

Fig. 7: Comparison of experimental similitude response and the TNO EOM (a) 93 m depth (b 179 m depth

Comparing Fig. 6 and Fig. 7 shows that including the gas inertia effects in the TNO EOM results in negligible differences in the gas bubble behaviour at the depth considered. These figures also show that the energy loss inherent within these models is not sufficient compared to the similitude plus energy loss or experimentally fit results.

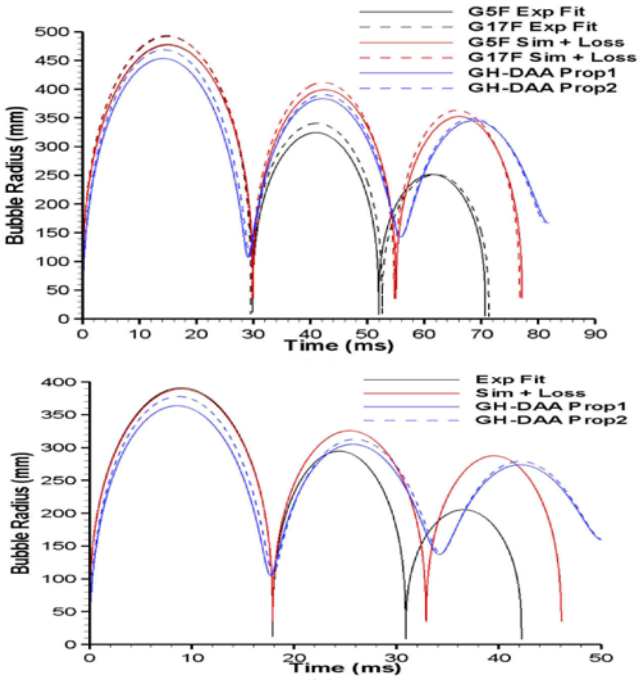

Fig. 8: Comparison of experimental similitude response and the GH-DAA EOM (a) 93 m depth (b) 179 m depth

The compressible fluid models over predict the radius by 27 and 54 percent for the second and third gas bubble maximums and the periods by 11 and 19 percent compared to the experimental fit results.

Fig. 8 shows that the energy loss inherent within the DAA EOM formulation produces slightly better bubble radius results than that shown by the Lamb EOM and significantly better results than the other compressible fluid models. The bubble period predicted by the DAA EOM is not as large as that imposed by the energy loss function however it is larger than that produced by the other compressible fluid analytical models.

In general the two property sets have only a minor effect on the later bubble cycles, as shown by the convergence of the time histories during the third bubble cycle.

6. CONCLUSIONS

An extensive study on the analytical equations of motion available for predicting the gas bubble behaviour was conducted to determine which models and assumptions provide better predictions. Using Mat LAB the various analytical models and similitude equations, a code was developed. It is also apparent that the energy loss inherent in the compressible fluid models does not fully predict the energy loss observed in experiments. The percent error in the gas bubble period and maximum bubble radius, compared to the experimental fits for a detonation depth of approximately

93 m and over 150 m, are shown in Table 3 and Table 4 respectively. The compressible EOM columns are the average of the various models that consider only compressibility in the surrounding fluid.

Table 3: Percent error in the gas bubble periods and maximum radii predicted by the analytical models compared to the experimental fits for a detonation depth of approximately 93 m

Cycle Number	Lamb EOM (%)		Compressible EOM		GH-DAA EOM (%)	
	Period	Radius	Period	Radius	Period	Radius
1st	1.32	1.64 4	1.01	1.60	1.39	6.59
2nd	3.10	22.3	10.9	27.1	6.78	15.45
3rd	6.47	41.5	19.6	54.5	15.2	37.2

Table 4: Percent error in the gas bubble periods and maximum radii predicted by the analytical models compared to the experimental fits for a detonation depth of over 150 m

Cycle Number	Lamb EOM (%)		Compressible EOM		GH-DAA EOM (%)	
	Period	Radius	Period	Radius	Period	Radius
1st	1.01	1.19	1.86	1.75	1.24	7.01
2nd	5.33	11.3	14.2	14.3	10.6	3.55
3rd	8.13	39.7	22.8	50.2	19.1	33.2

As these numbers show the Lamb EOM predicts the bubble period closer to the experimental fits than the other models. This shows that the energy loss function provides a larger loss than those inherent within the compressible fluid and GH-DAA EOM. As would be expected the GH-DAA model which accounts for fluid and gas bubble compressibility shows a significantly larger energy loss than the EOM considering compressibility in the fluid.

Table 3 and Table 4 show that there is a requirement to include an energy loss function in conjunction with the compressible fluid models. All models that include only the compressibility in the fluid produce results very similar to one another; therefore a single energy loss function could be developed for all of these models. A method that is proposed by Geers and Hunter involves starting from a time shortly after detonation, and involves determining the bubble growth during the shock-wave phase. This approach allows for the use of the gas constant determined from the equations of state to be used for the compressible gas models. This approach will be introduced into the models in the future.

7. ACKNOWLEDGEMENT

The work presented in this paper would not been possible without the support that I received from my supervisor Prof. KaushikBandyopadhyay. I am thankful to the Department of Construction Engineering, Jadavpur University for providing me with the facilities needed for the completion of my project.

REFERENCES

[1] Cole, R.H. (1948), Underwater Explosions, Princeton University Press, Princeton, 437.

[2] Geers, T.L., and Hunter, K.S. (2002), An integrated wave-effects model for an underwater explosion bubble, *J. Acoust. Soc. Am.*, 111 (4), 1584-1601.

[3] Herring, C. (1941), 'Theory of the pulsation of the gas bubble produced by an underwater explosion, in *Underwater Explosion Research* (Office of Naval Research, Washington, D.C., 1950), Vol. 2, 35-131.

[4] Jones, H., and Miller, A.R. (1948), 'The detonation of solid explosives', *Proc. R. Soc. London*, Ser. A 194A, 480-507.

[5] Kirkwood, J.G., and Bethe, H. (1942), 'The pressure wave produced by an underwater explosion I. (OSRD no. 588)' in *Shock and Detonation Waves*, edited by W.W. Wood (Gordon and Breach, New York, 1967), 1-34.

[6] Keller, J.B., and Kolodner, I.I. (1956), 'Damping of underwater explosion bubble oscillations', *J. Applied Phys.*, 27, 1152-1161.

[7] Lamb, H. (1923), 'The early stages of a submarine explosion', Philos. Mag., 45 (Ser 6), 257-265.

[8] Swift, E., and Decius, J.C. (1948), 'Measurements of bubble pulse phenomena III. Radius and period studies' in *Underwater Explosion Research* (Office of Naval Research, Washington, D.C., 1950), Vol. 2, 553-599.

[9] Van Aanhold, J.E. (2010), Simplified models for close-proximity UNDEX, TNO-034-DTM- 2009-04888, TNO report, CONFIDENTIAL.